Full Paper
doi.org/10.1002/chem.202004944

Chemistry Europe
European Chemical Societies Publishing

Organophosphate Removal

Paraoxonase Mimic by a Nanoreactor Aggregate Containing Benzimidazolium Calix and L-Histidine: Demonstration of the Acetylcholine Esterase Activity

Amanpreet Singh,[a] Sanjeev Saini,[a] Mayank,[a] Navneet Kaur,*[b] Ajnesh Singh,[c] Narinder Singh,*[a] and Doo Ok Jang*[d]

Abstract: An anion-mediated preorganization approach was used to design and synthesize the benzimidazolium-based calix compound **R1**·2ClO_4^-. X-ray crystallography analysis revealed that the hydrogen-bonding interactions between the benzimidazolium cations and *N*,*N*-dimethylformamide (DMF) helped **R1**·2ClO_4^- encapsulate DMF molecule(s). A nanoreactor, with **R1**·2ClO_4^- and L-histidine (L-His) as the components, was fabricated by using a neutralization method. The nanoreactor could detoxify paraoxon in 30 min. L-His played a vital role in this process. Paraoxonase is a well-known enzyme used for pesticide degradation. The Ellman's reagent was used to determine the percentage inhibition of the acetylcholinesterase (AChE) activity in the presence of the nanoreactor. The results indicated that the nanoreactor inhibited AChE inhibition.

Introduction

The increasing global hunger index has put the agriculture sector under pressure to produce more crops. However, increased crop production cannot be achieved without the use of pesticides.[1–3] There are numerous pesticides that do not degrade even after a considerable time has passed since its application and that cause serious health concerns.[4–7] The commonly known non-degradable pesticides are the organophosphates (OPs) and carbamates, which are the most prevalent toxic chemicals.[8–12] Acetylcholinesterase (AChE) hydrolyzes acetylcholine into choline, which plays a key role in maintaining the proper functioning of the peripheral cholinergic system. The inhibition of AChE activity induces the accumulation of acetylcholine, thereby resulting in the disruption of metabolism, which can eventually cause death.[13–17] The AChE activity is inhibited when its active site, serine, binds to the OPs (Scheme 1). The OPs that bind irreversibly to AChE through serine residues are more harmful than carbamate-based pesticides that bind reversibly to a target enzyme.[18–23]

Moreover, the OPs are employed as chemical warfare agents (CWAs) and are the major components of the nerve gases.[24,25] Therefore, to reduce pesticide poisoning (for sustainable development) and produce antidotes for CWAs, it is desirable to develop a highly efficient catalyst that can rapidly hydrolyze the OPs and detoxify them.[26–28] The hydrolysis of the OPs affords compounds incapable of phosphorylating the serine residue of AChE.

The complete removal of OPs from the environment and, ultimately, from food is challenging because most OPs are stable over a wide pH range.[29,30] The enzyme paraoxonase is well-known for its ability to hydrolyze various OPs. Paraoxonase possesses two histidine residues (His 115 and 134) in its structure, which are involved in proton transfer. The asparagine residue present in this enzyme stabilizes the intermediates at the active site.[31–33] However, the isolation of such enzymes is challenging. Hence, they cannot be used for the large-scale degradation of pesticides.

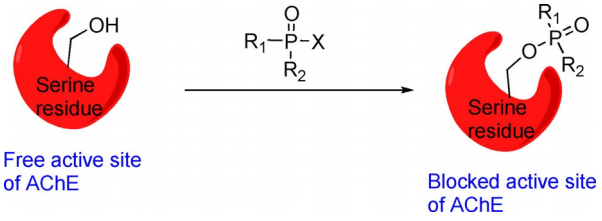

Scheme 1. Schematic representation of AChE inhibition by OPs.

[a] A. Singh, S. Saini, Mayank, Dr. N. Singh
Department of Chemistry, Indian Institute of Technology Ropar
Roopnagar, Punjab 140001 (India)
E-mail: nsingh@iitrpr.ac.in

[b] Dr. N. Kaur
Department of Chemistry, Panjab University, Chandigarh 160014 (India)
E-mail: navneetkaur@pu.ac.in

[c] A. Singh
Department of Applied Sciences & Humanities
Jawaharlal Nehru Govt. Eng. College, Sundernagar 175018 (India)

[d] Dr. D. O. Jang
Department of Chemistry, Yonsei University
Wonju 26493 (Republic of Korea)
E-mail: dojang@yonsei.ac.kr

Supporting information and the ORCID identification number(s) for the author(s) of this article can be found under: https://doi.org/10.1002/chem.202004944.

Although metal-based catalysts that can hydrolyze OPs have been reported, the use of expensive metals,[34–36] reduced efficiency of the catalysts (through hydration of the metal center in aqueous media), and poor biocompatibility limit their practical application. Farha and co-workers developed a zirconium-based metal–organic framework, which encapsulates OPs and hydrolyzes them to produce non-toxic phosphates.[26] It was reported that the catalyst system should bear highly active substituents attached to the metal complex to function efficiently in an aqueous medium. A nickel complex and a copper-based polymer that can sense OPs have also been reported.[37] Although these compounds could detect OPs, the metal complexes dissociated when they interacted with the OPs. This eventually led to low catalytic efficiencies (for the degradation of OPs). Furthermore, the mechanism of catalytic degradation of CWAs has been explained by an aggregation-based deactivation mechanism.[38]

Herein, we have explored the ionic interactions between anionic surfactants and benzimidazolium-based organic cations to develop micelle-type aggregates for use as catalysts. We hypothesized that the ionic liquid (IL)-based catalysts could potentially overcome the limitations posed by metal-based catalysts toward the hydrolysis of OPs as the imidazolium moieties in the ILs exhibit high phosphate ion affinities.[39–45]

Herein, we have developed a strategy for the in situ development of a nanoreactor, from benzimidazolium-based cationic calix and L-histidine (L-His) units, having all the essential catalyst parameters for the degradation of OPs. An anion-induced preorganization approach was used to synthesize the benzimidazolium-based calix unit. The cationic benzimidazolium moiety could interact with the L-His residue via ionic interactions and form a self-assembled nanoreactor. Both the units of the nanoreactor play crucial roles in facilitating the catalytic activity of the nanoreactor toward the hydrolysis of OPs. The benzimidazolium ring is known to hydrogen bond with electron-rich species and is widely used to activate electrophiles that participate in nucleophilic substitution reactions. L-His participates in enzyme catalysis and activates nucleophiles by abstracting protons.[46] The L-His residue of paraoxonase plays a crucial role during pesticide degradation.[31] Although ILs have been prevalently used in catalysis,[47–50] to the best of our knowledge, this is the first report of an aggregate nanoreactor containing benzimidazolium calix and L-His units that can degrade harmful pesticides.

Results and Discussion

Synthesis and characterization of the calix R1·2 ClO_4^-

The nucleophilic substitution reaction between compound **1**[50] and benzimidazole, in the presence of K_2CO_3, afforded compound **2** (Scheme 2). The structure of compound **2** was confirmed by using ^{1}H NMR spectroscopy and ^{13}C NMR spectroscopy techniques. The ^{1}H NMR spectrum exhibited a singlet at 4.5 ppm (corresponding to the four aliphatic methylene protons), indicating the attachment of the benzimidazole moiety to the mesitylene unit. Another singlet at 10.7 ppm (C–H,

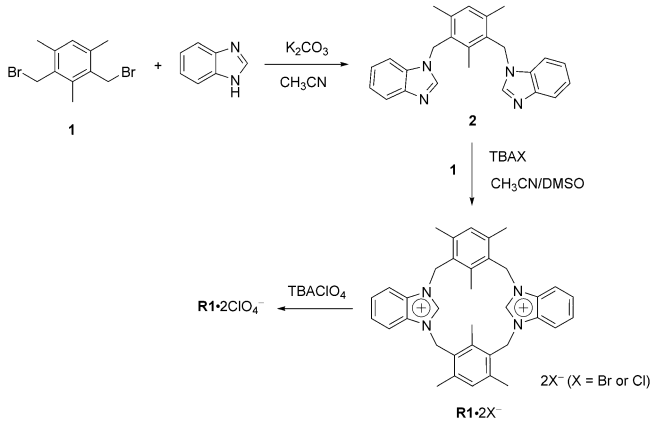

Scheme 2. Synthetic scheme for preparing benzimidazolium-based calix **R1**·2 ClO_4^-.

benzimidazole) validated the formation of compound **2**. The calix **R1**·2 X^- was subsequently prepared by using the anion-induced preorganization approach. The anions are known to induce the formation of a particular isomer of the reactants, leading to the exclusive production of the desired product.[51,52] Compound **2** exists in different steric orientations, all of which can potentially lead to the formation of different products. In such a scenario, the isolation of the products becomes challenging. Therefore, tetrabutylammonium (TBA) halides (TBAXs) were added to the reaction mixture to reorganize compound **2** for the exclusive formation of one calix compound. Among all the TBAXs used for the reaction, the use of TBACl resulted in the maximum yield of the calix **R1**·2 X^- compound. This is because the cavity formed by the organized benzimidazole-based dipodal compound **2** could suitably bind to the chloride anion through hydrogen bonding.[53] To further validate the role of the chloride ion in the synthesis of the calix **R1**·2 Cl^-, the reaction was performed by using different concentrations of TBACl. The progress of the reaction is presented in Figure 1.

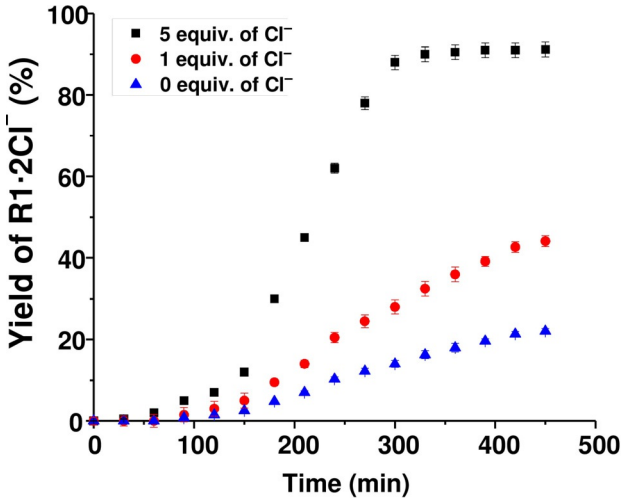

Figure 1. Variation in the yields of the calix **R1**·2 Cl^- versus time at different chloride ion concentrations.

The Calix **R1**·2 Cl^- was obtained in 90% yield when five equivalents of TBACl were used, and the reaction was allowed to proceed for 300 min. In the absence of TBACl, the calix **R1**·2 Cl^- compound was obtained in 20% yield. Interestingly, with five equivalents of the chloride ions, the desired product separated out as a white solid in acetonitrile. Side products were not formed. The chloride ions were replaced by ClO_4^- ions to grow crystals suitable for carrying out single-crystal X-ray diffraction (XRD) experiments. The calix **R1**·2 Cl^- was dissolved in H_2O/DMF (9:1, v/v) and 10 equivalents of $TBAClO_4$ were added to the solution. After boiling, the solution was cooled down to room temperature to yield white crystals of the calix **R1**·2 ClO_4^-, which were suitable for single-crystal XRD analysis.

Structural description of the calix R1·2 ClO_4^-

The crystal structure analysis revealed that the calix **R1**·2 ClO_4^- molecule crystallized in the tetragonal crystal system (space group: $I4_1/acd$, Table 1). The crystal consisted of one calix molecule, two ClO_4^- counterions, and two DMF molecules of crystallization. The packing of calix **R1**·2 ClO_4^- has not been extensively discussed as the ClO_4^- and DMF molecules were disordered. Selected bond lengths and angles are presented in Table S1 (in the Supporting Information). The ORTEP diagram and the atom numbering scheme for the calix **R1**·2 ClO_4^- is shown in Figure 2A. The packing diagram of the calix **R1**·2 ClO_4^- is shown in Figure 2B, which reveals that the mesitylene rings of the two calix molecules are oriented in a face-to-face manner, whereas the benzimidazolium rings remain outside.

Table 1. Crystal data and refinement parameters of the calix **R1**·2 ClO_4^-.

Parameters	**R1**·2 ClO_4^-
empirical formula	$C_{42}H_{52}Cl_2N_6O_{10}$
formula weight	871.80
T [°C]	20(2)
crystal system	tetragonal
space group	$I4_1/acd$
a [Å]	20.5860(9)
b [Å]	20.5860(9)
c [Å]	40.0136(16)
α [°]	90
β [°]	90
γ [°]	90
V [Å^3]	16957.1(12)
Z	16
D_c [Mgm^{-3}]	1.366
μ [mm^{-1}]	0.218
reflections collected	236852
data/restraints/parameters	4175/0/332
unique reflections, [R_{int}]	4175 [0.0714]
GOF = S_{all}	1.040
final R indices	
R_1, wR_2 [$I > 2\sigma I$]	0.0779, 0.2193
R_1, wR_2 (all data)	0.0888, 0.2270
$\Delta\rho_{max}/\Delta\rho_{min}$ [Å^3]	1.017/−1.077

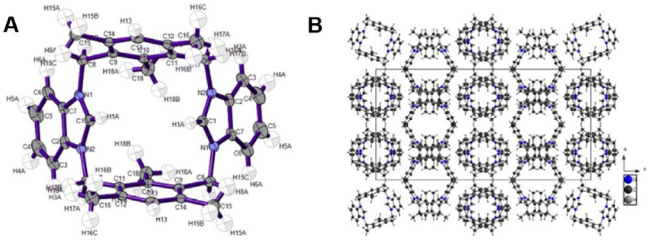

Figure 2. (A) ORTEP diagram and the atom numbering scheme for the calix **R1**·2 ClO_4^- with thermal ellipsoids drawn at the 40% probability level (for clarity, the disordered ClO_4^- and solvent molecules of crystallization are not shown). (B) Packing image of calix **R1**·2 ClO_4^- viewed down the *b*-axis.

Nanoreactor fabrication: in situ formation of aggregates from ionic conjugates formed of the benzimidazolium calix R1 and L-His

The ionic conjugates of the benzimidazolium calix **R1** and L-His were prepared by replacing the ClO_4^- ions in the calix **R1**·2 ClO_4^- with hydroxides.[54] Subsequently, the hydroxide ions were replaced with L-His (Figure 3A).[55,56] The resulting L-His anions formed an anionic conjugate with the benzimidazolium cation. The intermolecular hydrogen bonding L-His residues of the aggregates and the blockage of the hydrophilic

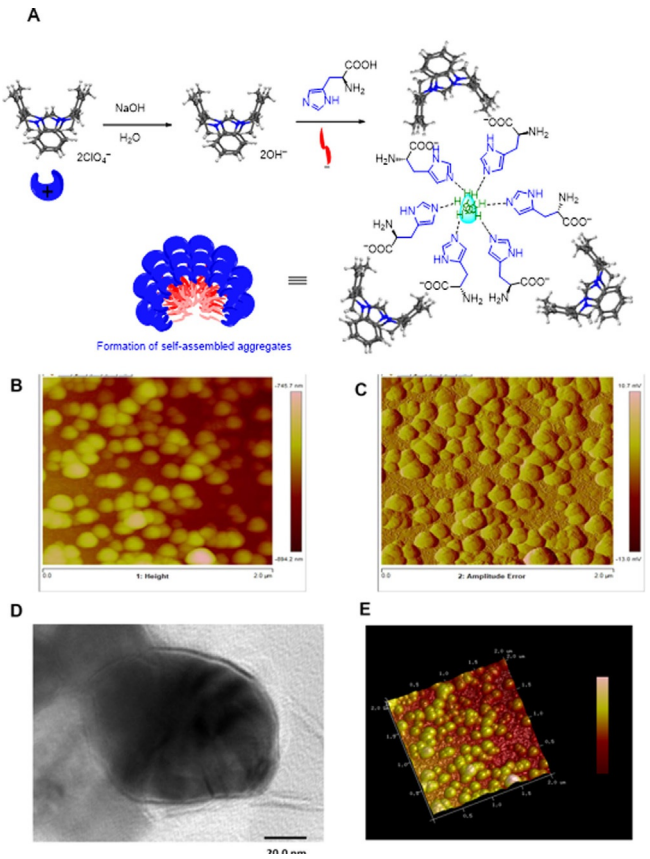

Figure 3. (A) Formation of self-assembled aggregates from the ionic conjugate of the calix **R1**·2 ClO_4^- and L-His. AFM images of the aggregates: (B) spherical aggregates; (C) amplitude error image of spherical aggregates; (D) TEM image of aggregates (100 nm); (E) 3D view of spherical aggregates.

core of the ionic conjugate (by the hydrophobic aromatic rings of the benzimidazolium moiety, leading to reduced solubility), can potentially explain the formation of the aggregates. Interestingly, when two equivalents of L-His were added to a clear solution of the calix **R1**·2OH^-, the solution became turbid. The turbidity was due to the formation of aggregates, as observed by dynamic light scattering (DLS) experiments (Figure S1 in the Supporting Information). It was reported that the aggregates were used as sensors and catalysts.[57–61] High-resolution images of the aggregates were recorded by using the atomic force microscopy (AFM) technique to investigate the sizes and morphologies of the aggregates (Figure 3B,C). The images revealed the aggregation of spherical particles having a radius of 172 nm. A transmission electron microscopy (TEM) image was also obtained with the size of aggregates of about 100 nm (Figure 3D).

The properties of the self-assembled aggregates formed from the ionic conjugates of the calix **R1**·2ClO_4^- and L-His were investigated by using the diffusion-ordered NMR spectroscopy (DOSY) technique. DOSY allows non-invasive detection of self-aggregation in the solution phase. The diffusion coefficient of the solute species can also be estimated by using this technique. The DOSY spectrum of **R1**·2ClO_4^- was recorded and the diffusion coefficient (D) was determined to be 1.55×10^{-10} m^2s^{-1} (Figures S2 and S3 in the Supporting Information). After the addition of an adequate amount of L-His, the DOSY spectrum was recorded again. Analysis of the spectrum revealed that upon the addition of L-His, the value of the diffusion coefficient (D) decreased to 1.35×10^{-10} m^2s^{-1} (Figures S4 and S5 in the Supporting Information). The results confirmed aggregation.

Degradation of paraoxon

It is known that AChE reacts with OPs via the L-His residue, which otherwise does not react with the OPs.[62,63] Various supramolecular interactions helped encapsulate the OPs in the cavity of AChE. These interactions enhanced the reactivity of the OPs by increasing the electrophilicity of the phosphate center.

Raushel et al. reported the role of phosphodiesterase in the hydrolysis of OPs.[64,65] Phosphodiesterase is a zinc-containing enzyme that hydrolyzes the P–O bond. The binding of OPs to the metal ions facilitates a nucleophilic attack on the phosphorus center, which favors the formation of a weak P–O bond, resulting in the eventual hydrolysis of the P–O bond. To date, zinc and zirconium complexes have been used for the hydrolysis of P–O bonds in phosphodiesters.[66–68] We have attempted to replace these metal ions with organic cationic receptors.

Initially, the conversion of paraoxon to *p*-nitrophenol was achieved by using the calix **R1**·2OH^- as a catalyst in the presence of a cocatalyst (Scheme 3). The ionic conjugates of the calix **R1**·2OH^- and/or the cocatalysts (0.1 equivalent) were dispersed in an aqueous medium, following which paraoxon was added to the solution. The degradation of paraoxon was monitored by recording the absorbance spectra of the solution at 412 nm (λ_{max} of *p*-nitrophenol). None of the catalysts, cocatalysts, substrates, and byproducts exhibited an absorbance maxima that was >380 nm. Therefore, they could not potentially interfere with the degradation of paraoxon. Catalytic studies revealed that neither the calix **R1**·2OH^- nor the cocatalyst could independently facilitate significant conversion of paraoxon to *p*-nitrophenol. However, the self-assembled aggregates facilitated the conversion of paraoxon (>80% efficiency) to the less-toxic products in 25 min (Figure 4A,B). The calibration plot (absorbance intensity vs. time, Figure 4C) was linear. The calculated half-life ($t_{1/2}$) of the catalyst was 6.9 min (Figure S6 in the Supporting Information). The catalytic activities of the calix **R1**·2OH^- were examined in the presence of other cocatalysts. The percentage of paraoxon degradation was significantly high when L-His was used as the cocatalyst (compared with other cocatalysts such as triethylamine, diethylamine, asparagine, piperidine, and imidazole, Figure S7 in the Supporting Information). The turnover number (K_{cat}) was calculated at different catalyst equivalents. The value of K_{cat} increased continuously when the catalyst amount was ≤0.1 equivalent. A stable K_{cat} value was reached at higher catalyst concentrations (Figure S8 in the Supporting Information). The degradation of OPs, such as paraoxone methyl, parathion, and parathion methyl was studied by using the nanoreactor. Similar catalytic activities were observed in the reaction involving paraoxon (Figure 5).

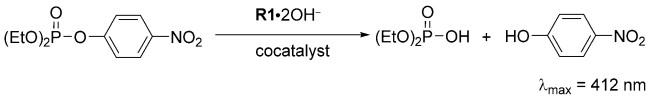

Scheme 3. Degradation of paraoxon in the presence of the fabricated catalytic nanoreactor using benzimidazolium-based calix **R1**·2HO^- (0.1 equivalent) and a cocatalyst (0.1 equivalent).

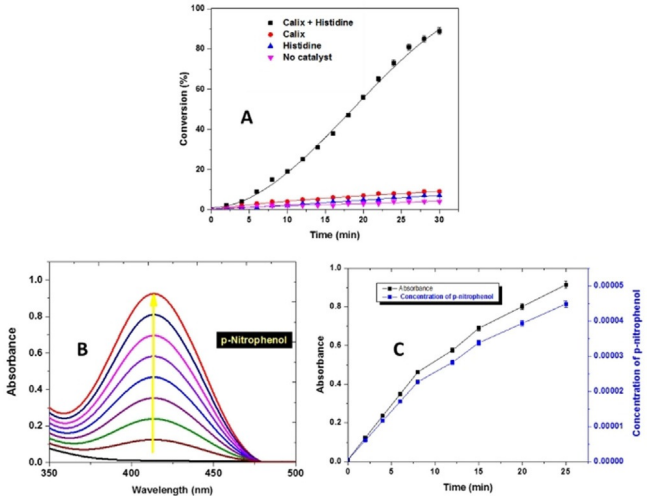

Figure 4. (A) Chart of the degradation of paraoxon at different catalytic conditions. (B) Change in the absorbance spectra of the solution of paraoxon (50 μM) and calix **R1**·2ClO_4^- (0.1 equivalent) in the presence of L-His (0.1 equivalent) with respect to time. (C) A calibration plot of the variation in absorbance with time.

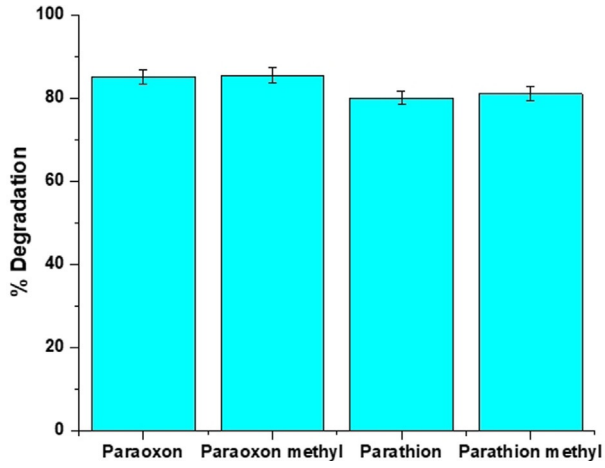

Figure 5. Percent degradation of different OPs in the presence of the nanoreactor. OPs (50 μM) were used with 0.1 equivalent (5 μM) of the nanoreactor. Reaction time: 25 min.

Hypothesized mechanism of paraoxon degradation

A hypothesized mechanism for the degradation of paraoxon is presented in Scheme 4. The single-crystal structure of the calix **R1**·2 ClO_4^- reveals that the cavity formed by the calix can encapsulate the paraoxon molecule through hydrogen bonding, leading to the enhanced electrophilic character of the phosphates. L-His acts as a base, which increases the nucleophilicity of water, thus facilitating the reaction. The conversion of paraoxon to diethyl phosphate increases the hydrophilicity of the cavity, resulting in the removal of diethyl phosphate from the benzimidazolium cavity. This creates a vacant site for another catalytic cycle. The ^{31}P NMR spectrum of paraoxon was recorded in the presence of the catalytic system to elucidate the nature of the interaction present between the calix unit and paraoxon (Figure S9 in the Supporting Information). The ^{31}P NMR signal corresponding to the phosphorous unit in paraoxon split into two peaks in the presence of the calix unit, confirming the interactive association between paraoxon and the calix unit in the catalytic system, which results in the hydrolysis of paraoxon.

To determine the binding affinity of the phosphate esters for cyclic bis-cations, ^1H NMR titration was performed. Diethyl chlorophosphate was chosen instead of aromatic organophosphate to eliminate the interference caused by aromatic protons. The imidazolium proton (C–H), which is highly acidic compared with other protons, readily interacts with organophosphate. Upon the addition of a diethylchlorophosphate, the singlet at 7.82 ppm (corresponding to the imidazolium C–H proton) shifted to 9.74 ppm (Figure S10 in the Supporting Information). The binding constant was calculated to be $4.36\times10^4\ M^{-1}$ (Figure S11 in the Supporting Information).[69]

Quantitative investigation of AChE activity

The Ellman's assay was performed to investigate the percentage of inhibition of AChE in the presence of the fabricated catalyst (Scheme 5). Instead of paraoxon, diethylchlorophosphate and diethylcyanophosphate (both devoid of nitro functionalities), that exhibit similar reactivities, were used for the studies. The Ellman's reagent, DTNB (5,5′-dithiobis-(2-nitrobenzoic acid), a chromogen), contains an S–S bond and an aromatic nitro group. The reagent reacts with a free thiol group to cleave the S–S bond, releasing 5-thio-2-nitrobenzoic acid (TNB), which exhibits a strong absorbance band at 412 nm. The concentration of the free thiol group was monitored by the ultraviolet-visible (UV/Vis) absorption spectroscopy technique. A solution of the OPs (50 μM), such as diethylchlorophophate and diethylcyanophophate, in the presence of the nanoreactor (0.1 equivalent) and the self-assembled aggregates, was stirred for 30 min. At every 2 min, an aliquot of the solution was collected and incu-

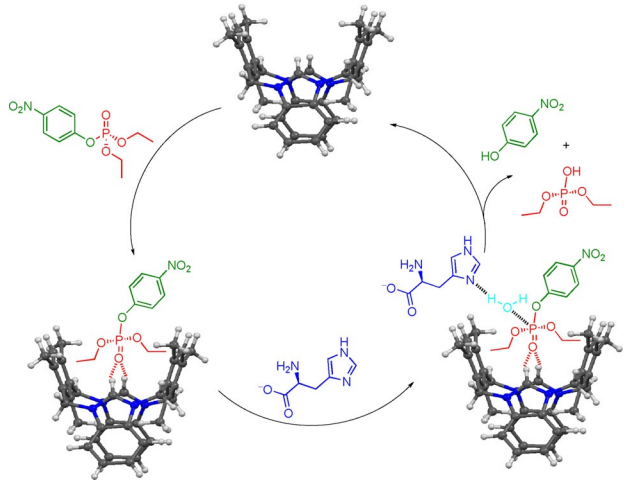

Scheme 4. Hypothesized mechanism of the degradation of paraoxon by the nanoreactor, the self-assembled aggregates of the ionic conjugate of the calix **R1**·2 OH^- and L-His.

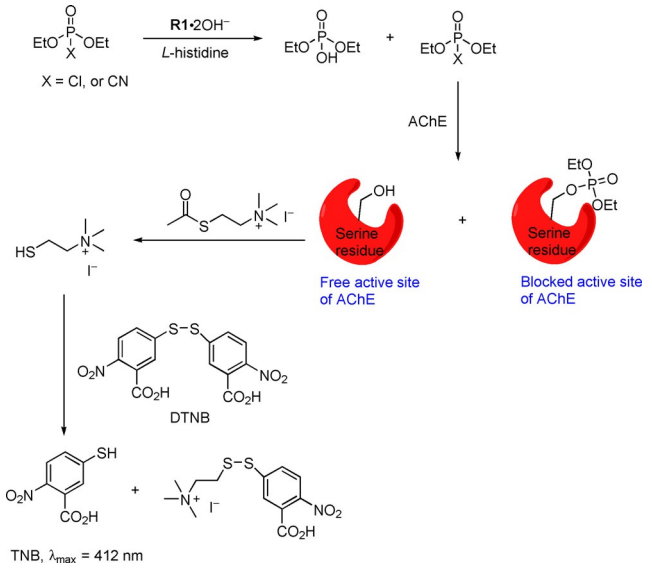

Scheme 5. AChE inhibition resistance owing to the hydrolysis of OPs and the principal reactions of Ellman's assay for the colorimetric determination of AChE activity.

bated with a known concentration of AChE. Following this, the solution was incubated with acetylthiocholine. Although some amounts of AChE were inhibited by the OPs, the activated AChE catalyzed the hydrolysis of acetylthiocholine. The AChE activity was evaluated by monitoring the concentration of thiocholine released during the hydrolysis reaction (using Ellman's reagent). The concentration of the released thiocholine should potentially be directly proportional to the efficiency of the catalyst. AChE inhibition was plotted with respect to time. The nanoreactor detoxicated the OPs within 30 min (Figure 6). It has been reported that β-cyclodextrin-oxime derivatives detoxicated OPs in the presence of 500 equivalents of the catalyst. A comparable activity was achieved with 0.1 equivalent of the fabricated catalyst reported herein.[70] It is worth mentioning that the calix **R1**·2 OH^- or L-His moieties did not individually exhibit significant AChE inhibition abilities (Figures S12 and S13 in the Supporting Information).

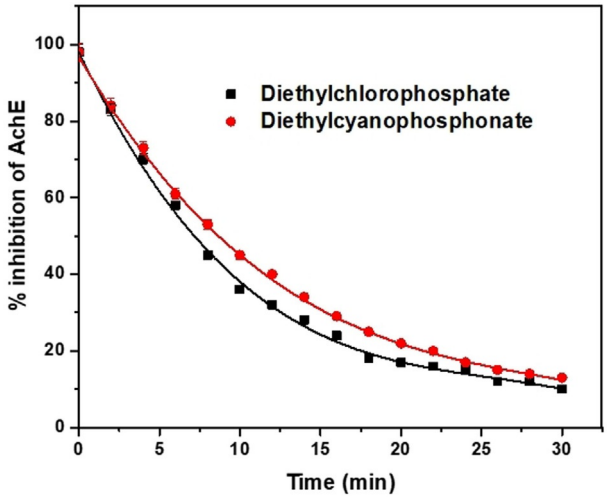

Figure 6. AChE inhibitory activity of diethylchlorophosphate and diethylcyanophosphate in the presence of the nanoreactor: OPs (50 μM) were used with 0.1 equivalent (5 μM) of the nanoreactor in a phosphate buffer (0.1 M, pH 7.8) at 37 °C.

Conclusion

A nanoreactor, formed of aggregates of an anionic conjugate of benzimidazolium calix and L-His residues, was developed. Because of the rigid cyclic structure (ionic in nature), the fabricated catalyst was highly stable. Furthermore, it was highly soluble in aqueous media. The catalyst could reversibly hydrogen bond to OPs and activate the electrophilic site of the phosphates, allowing a nucleophilic attack. The nanoreactor could degrade paraoxon and reactive CWAs with high efficiency. The developed nanoreactor could efficiently detoxify OPs and resist the inhibition of AChE. The catalytic activities of metal-based catalysts, toward the hydrolysis of numerous OPs, decrease in aqueous media. However, the new catalyst reported herein could be efficiently used for the degradation of OPs in aqueous media. Therefore, it can be used to detoxify organophosphates present in agricultural wastewater. The fabricated catalytic system is metal-free and less expensive compared with metal-based catalysts.

Experimental Section

General

All chemicals were purchased from Sigma–Aldrich Chemical Co. and used without further purification. The AChE enzyme, from *Streptomyces diastatochromogenes*, was purchased from Sigma–Aldrich. The ultraviolet-visible (UV/Vis) absorption spectra were recorded by using the Shimadzu UV-2600 spectrophotometer. For recording the ^{1}H NMR and ^{13}C NMR spectra, a JEOL spectrometer operating at 400 and 100 MHz, respectively, was used. The chemical shifts are expressed in ppm. Elemental analyses were conducted by using Fisons CHNS analyzers. The single-crystal X-ray diffraction (XRD) data were recorded at room temperature by using a Bruker X8 APEXIII KAPPA charge-coupled device (CCD) diffractometer. The intensities were measured by using graphite-monochromatized $Mo_{K\alpha}$ radiation ($\lambda = 0.71073$ Å). Scanning electron microscopy images were recorded with a JEOL JSM-6610LV instrument (voltage: 15 kV). AFM experiments were performed by using a Bruker AXS instrument (Model: Multimode 8). The particle size of the nanoparticles was determined by DLS experiments, employing the external probe feature of the Metrohm Microtrac Ultra Nanotrac particle size analyzer.

Synthesis of compound 1[71]

A solution of mesitylene (12 g, 0.10 mol), paraformaldehyde (6.15 g, 0.20 mol), and HBr (40 mL, 31 wt% HBr/acetic acid solution) in glacial acetic acid (50 mL) was stirred at 50 °C. After 3 h, distilled water (100 mL) was added to the reaction mixture, following which a white solid precipitated out. The reaction mixture was filtered, and the solid was collected. Subsequently, it was washed with water and air-dried to obtain compound **1** in 95% yield (29 g). ^{1}H NMR (400 MHz, $CDCl_3$): $\delta = 2.37$ (s, 6H, CH_3), 2.43 (s, 3H, CH_3), 4.55 (s, 4H, CH_2), 6.89 ppm (s, 1H, ArH); ^{13}C NMR (100 MHz, $CDCl_3$): $\delta = 14.8$, 19.6, 31.1, 130.8, 132.7, 137.3, 138.2 ppm; elemental analysis calcd (%) for $C_{11}H_{14}Br_2$: C 43.17, H 4.61, Br 52.22; found: C 43.06, H 4.53.

Synthesis of compound 2

A solution of anhydrous K_2CO_3 (414 mg, 3 mmol) and benzimidazole (236 mg, 2 mmol) was stirred in dry acetonitrile (100 mL) at 80 °C for 15 min. Subsequently, compound **1** (3.6 mg, 1 mmol) was added to the reaction mixture and the mixture was stirred for 10 h at 80 °C. The progress of the reaction was monitored by using the thin-layer chromatography technique. The solvent was evaporated and the obtained residue was purified by column chromatography on silica gel (eluent: *n*-hexane/EtOAc, 9:1) to obtain compound **2** in 88% yield (334 mg). ^{1}H NMR (400 MHz, [D_6]DMSO): $\delta = 2.13$ (s, 3H, CH_3), 2.30 (s, 6H, CH_3), 5.46 (s, 4H, CH_2), 7.15 (s, 1H, ArH), 7.20–7.23 (q, $J = 8$ Hz, 4H, bimiH), 7.45–7.47 (t, $J = 8$ Hz, 2H, bimiH), 7.65–7.67 (q, $J = 8$ Hz, 2H, bimiH), 7.78 ppm (s, 2H, 2-bimiH); elemental analysis calcd (%) for $C_{25}H_{24}N_4$: C 78.92, H 6.36, N 14.73; found C 78.84, H 6.30, N 14.66.

Synthesis of calix R1·2 Cl^-

A solution of compound **1** (303 mg, 1 mmol), **2** (380 mg, 1 mmol), and tetrabutylammonium chloride (TBACl, 1.4 g, 5 mmol) in dry acetonitrile (50 mL) was heated at reflux for 5 h under an argon at-

mosphere. Evaporation of the solvent afforded **R1**·2Cl$^-$ in 90% yield as a solid compound (615 mg). ^{1}H NMR (400 MHz, [D$_6$]DMSO): δ = 1.60 (s, 6H), 2.39 (s, 12H), 5.54 (d, J = 12 Hz, 4H), 5.73 (d, J = 12 Hz, 4H), 7.20 (s, 2H), 7.64 (s, 2H), 7.80 (q, J = 4 Hz, 4H), 8.27 ppm (q, J = 4 Hz, 4H); ^{13}C NMR (100 MHz, [D$_6$]DMSO): δ = 15.5, 20.5, 46.1, 114.6, 127.7, 127.9, 132.3, 132.9, 138.3, 138.7, 140.8 ppm; HRMS (ESI): m/z calcd for $(C_{36}H_{38}N_4)^{2+}$: 263.1543 $[M]^{2+}$; found: 263.1502.

Synthesis of calix R1·2 ClO_4^-

The calix **R1**·2Cl$^-$ (606 mg, 1 mmol) was dissolved in 30 mL of a mixed solvent system (H_2O/DMF, 9:1, v/v) and tetrabutylammonium perchlorate (TBAClO_4, 1.7 g, 5 mmol) was added to the solution. The mixture was heated at reflux for 4 h. **R1**·2ClO_4^- separated out as crystals when the reaction mixture was cooled down to room temperature. Elemental analysis calcd (%) for $C_{36}H_{38}N_4Cl_2O_8$: C 59.59, H 5.28, N 7.72; found: C 59.43, H 5.20, N 7.61.

XRD analysis of the calix R1·2 ClO_4^-

The XRD data of the calix **R1**·2ClO_4^- were recorded with a Bruker D8 Venture PHOTON 100 CMOS diffractometer at 20 °C using mirror monochromatized $Mo_{K\alpha}$ radiation (λ = 0.71073 Å). Diffraction patterns were collected at a detector distance of 50 mm from where the crystal was positioned (counting time: 10 s). Data reduction and multi-scan absorption were conducted by using the APEX II program suite (Bruker, 2007). The structure of the calix **R1**·2ClO_4^- compound was solved by using the SIR-92 program and full-matrix least-square refinement was performed by using the SHELXL-97 program.[72] All non-hydrogen atoms were refined anisotropically. The hydrogen atoms of the C–H groups were assigned isotropic parameters the values of which were 1.2 times greater than those of the corresponding non-hydrogen atoms to which they were attached. All other calculations were performed by using the WinGX and PARST programs. Molecular diagrams were drawn by using DIAMOND. The final R-values, together with the selected refinement details, are given in Table 1. Deposition number 1555450 contains the supplementary crystallographic data for this paper. These data are provided free of charge by the joint Cambridge Crystallographic Data Centre and Fachinformationszentrum Karlsruhe Access Structures service.

Fabrication of the nanoreactor

A solution of the calix **R1**·2ClO_4^- (724 mg, 1 mol) and NaOH (120 mg, 3 mmol) in a mixture of MeOH and DMF (40 mL, MeOH/DMF, 9:1, v/v) was heated at reflux for 4 h. The solids precipitated out when the reaction mixture was cooled down to room temperature. After washing the solid with MeOH, the calix **R1**·2HO$^-$ was obtained in 80% yield (434 mg). Following this, the calix **R1**·2HO$^-$ (54.3 mg, 0.1 mmol) was dissolved in water (20 mL) to afford a transparent solution. Subsequently, a solution of L-His (31 mg, 0.2 mmol) in water (25 mL) was added to the above solution to form the aggregates. The turbidity of the solution indicated the formation of aggregates.

Photophysical measurements for the hydrolysis of paraoxon

A solution of paraoxon in water (50 μM) was added to an aqueous solution of the calix **R1**·2OH$^-$ and L-His conjugate (each 5.0 μM). The solution was buffered at pH 7.8 using N-ethyl morpholine. The solution was shaken vigorously before the absorbance spectra were recorded after a short interval. The rate of hydrolysis was determined from the plot of ln(c) vs. time.

Analysis of AChE activity

The Ellman's solution was prepared by dissolving acetylthiocholine iodide (200 mg, 0.7 mmol), 5,5′-dithiobis-(2-nitrobenzoic acid) (DTNB; 100 mg, 0.175 mmol), and $NaHCO_3$ (50 mg) in a phosphate buffer (25 mL, 0.1 M, pH 7.8). The solution was diluted 10-fold. The activity of the residual AChE was determined by using a microplate reader (infinite M200PRO, TECAN).

Acknowledgments

This work was supported by a research grant from the SERB Project (Project No. EMR/2017/003438). A.S. is thankful to IIT Ropar for the institute's postdoctoral fellowship.

Conflict of interest

The authors declare no conflict of interest.

Keywords: acetylcholine esterase · calix · nanoreactors · organophosphates · paraoxonase · pesticides

[1] S. Qian, H. Lin, *Anal. Chem.* **2015**, *87*, 5395 – 5400.
[2] L. L. Wen, F. Wang, X. K. Leng, C. G. Wang, L. Y. Wang, J. M. Gong, D. F. Li, *Cryst. Growth Des.* **2010**, *10*, 2835 – 2838.
[3] H. Suzuki, M. Tomizawa, Y. Ito, K. Abe, Y. Noro, M. Kamijima, *J. Agric. Food Chem.* **2013**, *61*, 9961 – 9965.
[4] N. Wang, M. Huang, X. Guo, P. Lin, *Environ. Sci. Technol.* **2016**, *50*, 9627 – 9635.
[5] P. D. Mabbitt, G. J. Correy, T. Meirelles, N. J. Fraser, M. L. Coote, C. J. Jackson, *Biochemistry* **2016**, *55*, 1408 – 1417.
[6] J. Kalisiak, E. C. Ralph, J. R. Cashman, *J. Med. Chem.* **2012**, *55*, 465 – 474.
[7] R. Sharma, B. Gupta, T. Yadav, S. Sinha, A. K. Sahu, Y. Karpichev, N. Gathergood, J. Marek, K. Kuca, K. K. Ghosh, *ACS Sustainable Chem. Eng.* **2016**, *4*, 6962 – 6973.
[8] M. C. Dumlao, L. E. Jeffress, J. J. Gooding, W. A. Donald, *Analyst* **2016**, *141*, 3714 – 3721.
[9] A. K. Ghosh, M. Brindisi, *J. Med. Chem.* **2015**, *58*, 2895 – 2940.
[10] Q. A. T. Le, R. Chang, Y. H. Kim, *Chem. Commun.* **2015**, *51*, 14536 – 14539.
[11] B. Wang, H. Wang, X. Zhong, Y. Chai, S. Chen, R. Yuan, *Chem. Commun.* **2016**, *52*, 5049 – 5052.
[12] N. Fahimi-Kashani, M. R. Hormozi-Nezhad, *Anal. Chem.* **2016**, *88*, 8099 – 8106.
[13] G. Aragay, F. Pino, A. Merkoçi, *Chem. Rev.* **2012**, *112*, 5317 – 5338.
[14] Y. Miao, N. He, J.-J. Zhu, *Chem. Rev.* **2010**, *110*, 5216 – 5234.
[15] J. R. Tormos, K. L. Wiley, Y. Wang, D. Fournier, P. Masson, F. Nachon, D. M. Quinn, *J. Am. Chem. Soc.* **2010**, *132*, 17751 – 17759.
[16] I. Effects, *J. Am. Chem. Soc.* **2005**, *3*, 2 – 3.
[17] Y. Guo, T. Guo, V. A. Online, *Chem. Commun.* **2013**, *49*, 1073 – 1075.
[18] L. M. Eubanks, T. J. Dickerson, K. D. Janda, *Chem. Soc. Rev.* **2007**, *36*, 458 – 470.
[19] B. M. Smith, *Chem. Soc. Rev.* **2008**, *37*, 470 – 478.
[20] Y. Liu, M. Bonizzoni, *J. Am. Chem. Soc.* **2014**, *136*, 14223 – 14229.
[21] D. E. B. Gomes, R. D. Lins, P. G. Pascutti, C. Lei, T. A. Soares, *J. Phys. Chem. B* **2011**, *115*, 15389 – 15398.
[22] B. J. Lavey, K. D. Janda, *J. Org. Chem.* **1996**, *61*, 7633 – 7636.
[23] R. K. Sit, V. V. Fokin, G. Amitai, K. B. Sharpless, P. Taylor, Z. Radic, *J. Med. Chem.* **2014**, *57*, 1378 – 1389.
[24] Y. J. Jang, D. P. Murale, D. G. Churchill, *Analyst* **2014**, *139*, 1614 – 1617.
[25] K. Kim, O. G. Tsay, D. A. Atwood, D. G. Churchill, *Chem. Rev.* **2011**, *111*, 5345 – 5403.

[26] J. E. Mondloch, M. J. Katz, W. C. Isley III, P. Ghosh, P. Liao, W. Bury, G. W. Wagner, M. G. Hall, J. B. Decoste, G. W. Peterson, R. Q. Snurr, C. J. Cramer, J. T. Hupp, O. K. Farha, *Nat. Mater.* **2015**, *14*, 512 – 516.
[27] L. M. Zimmermann, G. I. Almerindo, J. R. Mora, I. H. Bechtold, H. D. Fiedler, F. Nome, *J. Phys. Chem. C* **2013**, *117*, 26097 – 26105.
[28] R. K. Totten, Y. S. Kim, M. H. Weston, O. K. Farha, J. T. Hupp, S. T. Nguyen, *J. Am. Chem. Soc.* **2013**, *135*, 11720 – 11723.
[29] M. R. Sambrook, J. R. Hiscock, A. Cook, A. C. Green, I. Holden, J. C. Vincent, P. a Gale, *Chem. Commun.* **2012**, *48*, 5605 – 5607.
[30] R. K. Totten, M. H. Weston, J. K. Park, O. K. Farha, J. T. Hupp, S. T. Nguyen, *ACS Catal.* **2013**, *3*, 1454 – 1459.
[31] D. Blaha-Nelson, D. M. Krüger, K. Szeler, M. Ben-David, S. C. L. Kamerlin, *J. Am. Chem. Soc.* **2017**, *139*, 1155 – 1167.
[32] G. Garai-Ibabe, M. Möller, V. Pavlov, *Anal. Chem.* **2012**, *84*, 8033 – 8037.
[33] M. Harel, A. Aharoni, L. Gaidukov, B. Brumshtein, O. Khersonsky, R. Meged, H. Dvir, R. B. G. Ravelli, A. McCarthy, L. Toker, I. Silman, J. L. Sussman, D. S. Tawfik, *Nat. Struct. Mol. Biol.* **2004**, *11*, 412 – 419.
[34] D. B. Dwyer, J. Liu, J. C. Gomez, T. M. Tovar, A. Davoodabadi, W. E. Bernier, J. B. Decoste, W. E. Jones, *ACS Appl. Mater. Interfaces* **2019**, *11*, 31378 – 31385.
[35] X. Liang, L. Han, *Adv. Funct. Mater.* **2020**, *30*, 2001931.
[36] H. Chen, R. Q. Snurr, *ACS Appl. Mater. Interfaces* **2020**, *12*, 14631 – 14640.
[37] P. Raj, A. Singh, K. Kaur, T. Aree, A. Singh, N. Singh, *Inorg. Chem.* **2016**, *55*, 4874 – 4883.
[38] N. Zhen, J. Dong, Z. Lin, X. Li, Y. Chi, C. Hu, *Chem. Commun.* **2020**, *56*, 13967 – 13970.
[39] Q.-S. Lu, L. Dong, J. Zhang, J. Li, L. Jiang, Y. Huang, S. Qin, C.-W. Hu, X.-Q. Yu, *Org. Lett.* **2009**, *11*, 669 – 672.
[40] Q. Cui, Y. Yang, C. Yao, R. Liu, L. Li, *ACS Appl. Mater. Interfaces* **2016**, *8*, 35578 – 35586.
[41] H. N. Lee, N. J. Singh, S. K. Kim, J. Y. Kwon, Y. Y. Kim, K. S. Kim, J. Yoon, *Tetrahedron Lett.* **2007**, *48*, 169 – 172.
[42] Y. Su, Y. Wang, X. Li, X. Li, R. Wang, *ACS Appl. Mater. Interfaces* **2016**, *8*, 18904 – 18911.
[43] D. Wang, D. H. De Jong, A. Rhling, V. Lesch, K. Shimizu, S. Wulff, A. Heuer, F. Glorius, H. J. Galla, *Langmuir* **2016**, *32*, 12579 – 12592.
[44] A. Kumar, A. Pandith, H. Kim, *Sens. Actuators B* **2016**, *231*, 293 – 301.
[45] P. Drücker, A. Ruhling, D. Grill, D. Wang, A. Draeger, V. Gerke, F. Glorius, H. J. Galla, *Langmuir* **2017**, *33*, 1333 – 1342.
[46] U. K. Sharma, N. Sharma, R. Kumar, R. Kumar, A. K. Sinha, *Org. Lett.* **2009**, *11*, 4846 – 4848.
[47] H. Sharma, N. Kaur, N. Singh, D. O. Jang, *Green Chem.* **2015**, *17*, 4263 – 4270.
[48] X. Cui, S. Zhang, F. Shi, Q. Zhang, X. Ma, L. Lu, Y. Deng, *ChemSusChem* **2010**, *3*, 1043 – 1047.
[49] P. Pavez, D. Milla, J. I. Morales, E. A. Castro, C. Lo, J. G. Santos, *J. Org. Chem.* **2013**, *78*, 9670 – 9676.
[50] A. Singh, P. Raj, A. Singh, J. J. Dubowski, N. Kaur, N. Singh, *Inorg. Chem.* **2019**, *58*, 9773 – 9784.
[51] R. Tepper, B. Schulze, H. Görls, P. Bellstedt, M. Jäger, U. S. Schubert, *Org. Lett.* **2015**, *17*, 5740 – 5743.
[52] E. A. Katayev, G. D. Pantos, M. D. Reshetova, V. N. Khrustalev, V. M. Lynch, Y. A. Ustynyuk, J. L. Sessler, *Angew. Chem. Int. Ed.* **2005**, *44*, 7386 – 7390; *Angew. Chem.* **2005**, *117*, 7552 – 7556.
[53] H. Türkmen, S. Denizalti, I. Özdemir, E. Çetinkaya, B. Çetinkaya, *J. Organomet. Chem.* **2008**, *693*, 425 – 434.
[54] K. Ohno, H. Fukumoto, *Acc. Chem. Res.* **2007**, *40*, 1122 – 1129.
[55] R. F. De Dupont, J. Consorti, C. S. Suarez, A. Z. Paulo, R. F. de Souza, *Org. Synth.* **2002**, *79*, 236.
[56] A. Singh, A. Singh, N. Singh, D. Ok, *Tetrahedron* **2016**, *72*, 3535 – 3541.
[57] D. C. González, E. N. Savariar, S. Thayumanavan, *J. Am. Chem. Soc.* **2009**, *131*, 7708 – 7716.
[58] T. Gunnlaugsson, *Nat. Chem.* **2016**, *8*, 6 – 7.
[59] J.-H. Zhu, C. Yu, Y. Chen, J. Shin, Q.-Y. Cao, J. S. Kim, H. Xie, S. Wu, D. Su, B. Kim, Y.-T. Chang, *Chem. Commun.* **2017**, *266*, 22887.
[60] R. Kumar, S. Sandhu, P. Singh, S. Kumar, *J. Mater. Chem. C* **2016**, *4*, 7420 – 7429.
[61] P. Singh, L. S. Mittal, V. Vanita, K. Kumar, A. Walia, G. Bhargava, S. Kumar, *J. Mater. Chem. B* **2016**, *4*, 3750 – 3759.
[62] G. W. Peterson, S. Y. Moon, G. W. Wagner, M. G. Hall, J. B. Decoste, J. T. Hupp, O. K. Farha, *Inorg. Chem.* **2015**, *54*, 9684 – 9686.
[63] M. M. Meier, C. Rajendran, C. Malisi, N. G. Fox, C. Xu, S. Schlee, D. P. Baroondeau, B. Höcker, R. Sterner, F. M. Raushel, *J. Am. Chem. Soc.* **2013**, *135*, 11670 – 11677.
[64] K. T. Lum, H. J. Huebner, Y. Li, T. D. Phillips, F. M. Raushel, *Chem. Res. Toxicol.* **2003**, *16*, 953 – 957.
[65] S. D. Aubert, Y. Li, F. M. Raushel, *Biochemistry* **2004**, *43*, 5707 – 5715.
[66] T. Islamoglu, A. Atilgan, S.-Y. Moon, G. W. Peterson, J. B. DeCoste, M. Hall, J. T. Hupp, O. K. Farha, *Chem. Mater.* **2017**, *29*, 2672 – 2676.
[67] Y. Liu, S. Y. Moon, J. T. Hupp, O. K. Farha, *ACS Nano* **2015**, *9*, 12358 – 12364.
[68] P. Li, S. Y. Moon, M. A. Guelta, L. Lin, D. A. Gomez-Gualdron, R. Q. Snurr, S. P. Harvey, J. T. Hupp, O. K. Farha, *ACS Nano* **2016**, *10*, 9174 – 9182.
[69] S. K. Chang, A. D. Hamilton, *J. Am. Chem. Soc.* **1988**, *110*, 1318 – 1319.
[70] R. Le Provost, T. Wille, L. Louise, N. Masurier, S. Müller, G. Reiter, P.-Y. Renard, O. Lafont, F. Worek, F. Estour, *Org. Biomol. Chem.* **2011**, *9*, 3026 – 3032.
[71] A. W. van der Made, R. H. Van der Made, *J. Org. Chem.* **1993**, *58*, 1262 – 1263.
[72] G. M. Sheldrick, *Acta Crystallogr. Sect. A* **2008**, *64*, 112 – 122.

Manuscript received: November 13, 2020
Accepted manuscript online: December 22, 2020
Version of record online: March 3, 2021